6262–6273 *Nucleic Acids Research, 2016, Vol. 44, No. 13* *Published online 10 May 2016*
doi: 10.1093/nar/gkw397

The progression of replication forks at natural replication barriers in live bacteria

M. Charl Moolman[1,†], Sriram Tiruvadi Krishnan[1,†], Jacob W.J. Kerssemakers[1], Roy de Leeuw[1], Vincent Lorent[2], David J. Sherratt[3] and Nynke H. Dekker[1,*]

[1]Department of Bionanoscience, Kavli Institute of Nanoscience, Faculty of Applied Sciences, Delft University of Technology, Lorentzweg 1, 2628 CJ Delft, The Netherlands, [2]Université Paris 13, Sorbonne Paris Cité, Laboratoire de Physique des Lasers, CNRS, (UMR 7538), F-93430 Villetaneuse, France and [3]Department of Biochemistry, University of Oxford, Oxford OX1 3QU, UK

Received November 9, 2015; Revised April 27, 2016; Accepted April 28, 2016

ABSTRACT

Protein–DNA complexes are one of the principal barriers the replisome encounters during replication. One such barrier is the Tus–*ter* complex, which is a direction dependent barrier for replication fork progression. The details concerning the dynamics of the replisome when encountering these Tus–*ter* barriers in the cell are poorly understood. By performing quantitative fluorescence microscopy with microfuidics, we investigate the effect on the replisome when encountering these barriers in live *Escherichia coli* cells. We make use of an *E. coli* variant that includes only an ectopic origin of replication that is positioned such that one of the two replisomes encounters a Tus–*ter* barrier before the other replisome. This enables us to single out the effect of encountering a Tus–*ter* roadblock on an individual replisome. We demonstrate that the replisome remains stably bound after encountering a Tus–*ter* complex from the non-permissive direction. Furthermore, the replisome is only transiently blocked, and continues replication beyond the barrier. Additionally, we demonstrate that these barriers affect sister chromosome segregation by visualizing specific chromosomal loci in the presence and absence of the Tus protein. These observations demonstrate the resilience of the replication fork to natural barriers and the sensitivity of chromosome alignment to fork progression.

INTRODUCTION

All dividing cells must ensure the accurate and timely replication of their genome. The replication of DNA is an intricate process undertaken by the ubiquitous multi-protein complex known as the replisome (1–3). In *Escherichia coli*, the two independent replisomes (4) assemble at a single origin of replication (*oriC*) and subsequently advance in opposite directions at equal rates to synthesize the 4.6 Mbp genome, while the newly replicated DNA is sequentially segregated (5–9) prior to cell division. During fork progression, the replisomes encounter a substantial number of impediments preceding their fusion in the terminus region (10). Stalled replication forks are a potential source of genome instability, and thus a risk of cell viability in general (11). The major source of hindrance for a replisome during replication is believed to be protein–DNA complexes (12). A specific natural protein–DNA complex that is particularly involved in the termination of replication is the 36 kDa monomeric Tus protein bound to one of the ∼10 specific 23 bp DNA sequences (*ter*-sites) (13–16). The majority of these *ter* sequences are spread across the terminus region of the chromosome, spanning ∼2 Mbp across the two replichores (chromosome halves) (17) (Figure 1A). Replication forks are believed to be stalled when approaching such a Tus–*ter* complex from one direction (non-permissive side) but not from the other direction (permissive side) (18–22) (Figure 1B, top), creating a replication fork barrier (RFB). The dominant mechanism of forming such a RFB is thought to be the binding of a conserved G-C(6) base pair residue (Figure 1B, left) to Tus. Lock formation is formed through the separation of the parental DNA strand in the non-permissive direction by the replicative helicase (DnaB) until the conserved residue is free and subsequently binds to the binding pocket of Tus (Figure 1B, right) (23). Other lock formation mechanisms, for example protein–Tus interactions, have also been proposed (24), but seem unlikely to be the dominant mechanism (25). The binding of Tus to a *ter* site is strongly dependent on ionic strength (26). For example, Tus has a dissociation constant of $K_d \sim$ pM and a half-life of $t_{1/2} \sim 500$ min in 0.15 M potassium glutamate, while in 0.25 M potassium chloride

*To whom correspondence should be addressed. Tel: +31 15 2783219; Fax: +31 15 2781202; Email: n.h.dekker@tudelft.nl
†These authors contributed equally to the paper as first authors.

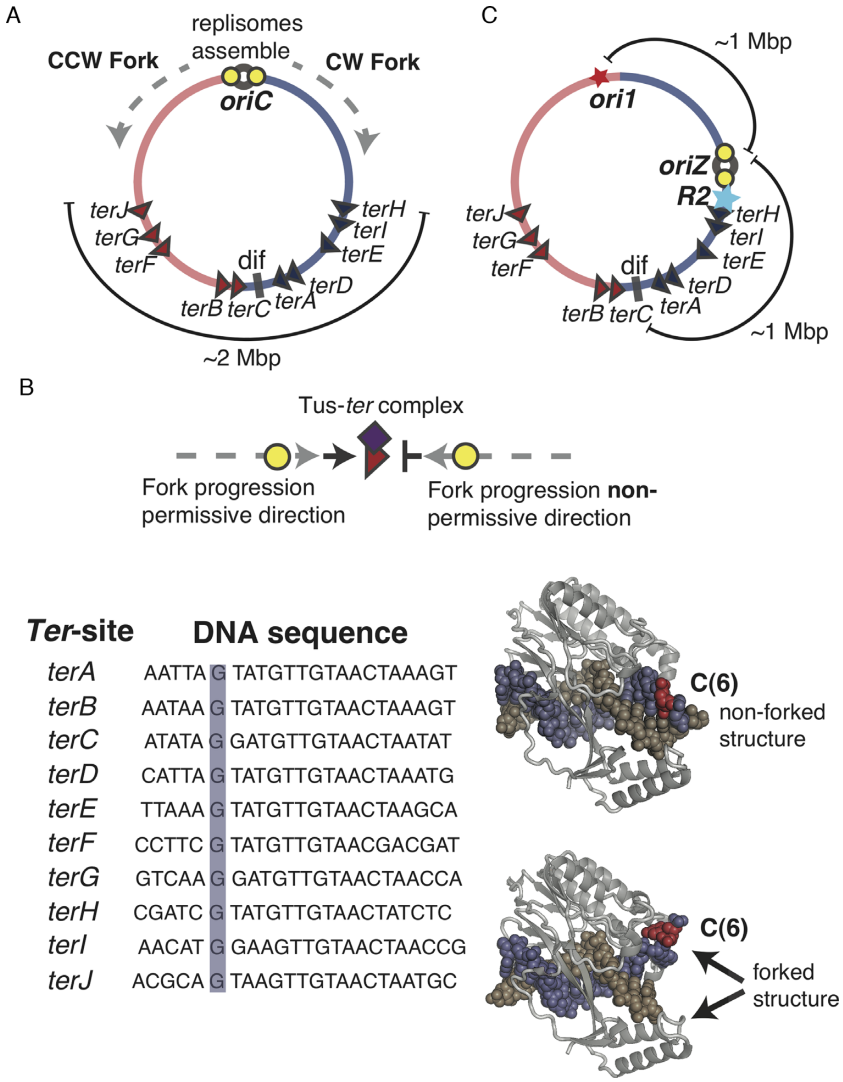

Figure 1. Investigating the Tus–*ter* replication block efficacy in an *Escherichia coli* strain with an ectopic origin. (**A** and **B**) The different *E. coli* chromosome arrangements. The left (red) and right replichore (blue), together with their respective *ter*-sites (triangles) are shown. The dashed gray lines indicate the directionality of the two independent replisome (yellow circles) movement. (A) The parental WT strain (oriC-dnaN-strain) which has roughly equal genomic distance from *oriC* till the innermost *ter*-sites for both replisomes. (B) Polar-fork arrest by the Tus–*ter* complex. (top) A schematic representation illustrating two replisomes approaching the permissive and non-permissive faces of a Tus–*ter* complex. The purple square represents the Tus protein. The replisome approaching from the non-permissive side is believed to be blocked by the Tus–*ter* complex indicated here with a flat arrowhead. (left, right) The dominant mechanism of polar fork arrest by a Tus–*ter* complex. (left) The DNA sequences of the different *ter*-sites. Here the conserved G is highlighted by a light blue rectangle. (right) The crystal structures of a non-forked Tus-bound *ter*-site and a forked Tus-bound *ter*-site approached from the non-permissive direction. Here the Tus protein is depicted in light gray. Images where generated using the Protein Data Bank (PDB) files, 1ECR and 2EWJ (23,66). DNA molecules are represented in purple and brown, while the C(6) residue is highlighted in red. (**C**) The strain with an ectopic origin (oriZ-dnaN-strain) (38). Here the origin of replication (*oriZ*) is positioned at 344 kb on the *E. coli* genetic map. The insertion position of a *lacO* operator array at 3908 kb (*ori1*), and a *tetO* operator array at 366 kb (*R2*) are indicated with a red and blue star respectively.

(KCl), it exhibits a $K_d \sim$ nM and a $t_{1/2} \sim 2$ min (27). In physiological ionic strength (150 mM KCl), the half-life for a Tus–*ter* locked complex was found to be $t_{1/2} \sim 500$ min (23). The RFB system is conserved in *Bacillus subtilis* (28–30), and has also been demonstrated to be capable of artificially pausing a replication fork in yeast and mammalian cells (31,32).

The biological significance of the Tus–*ter* RFB and the fate of a replisome when encountering such a barrier in live cells remains poorly understood (21). The 'replication fork trap' (RFT) model suggests that the Tus–*ter* complexes act as a safeguard, ensuring that forks can enter but not exit the inner termination zone, thereby restraining fork fusion to the zone roughly opposite the origin of replication (33). However, it is not clear why this would be necessary. It might assist fork fusion by ensuring that one of the two replisomes 'waits' for the other oppositely progressing replisome to complete replication, or reduce the incidence of head-on collisions between the replication and transcription machineries (10). It might also be related to the presence of the specific locus important for segregation (*dif*), situated between the innermost *ter*-sites (Figure 1A). The multiplic-

ity of *ter*-sites on each of the two chromosome arms suggests that a replication fork may, despite the strong DNA binding of Tus, frequently overcome a non-permissive Tus–*ter* roadblock. A bulk *in vivo* study of plasmid fork arrests (34) suggests that the different *ter*-sites have distinct fork arrest efficiencies, with the innermost sites (*terA-E*) being the most effective (20–35%). This is in line with an *in vitro* study that demonstrated that Tus binds strongly to *terA-E* and less strongly to other *ter*-sites (35). It remains unclear what happens to a replisome when it encounters such a block. Given the relatively low efficiencies of the RFBs and the *in vitro* robustness of the replisome in head-on collisions (36,37), it could be the case that the replisome remains intact after encountering a Tus–*ter* block, or rapidly restart and proceed further with replication.

To gain insight into the response of a replisome as it encounters a Tus–*ter* roadblock under *in vivo* conditions, we study single live *E. coli* cells that contain only an ectopic origin (38) in either the presence or absence of Tus (Figure 1C). The *oriZ* position is such that the clockwise (CW) replisome encounters a non-permissive Tus–*ter* complex earlier on in replication than the counterclockwise (CCW) replisome. The strain also includes a genomic rearrangement of a highly transcribed region (*rrnCABE* operon cluster) that alleviates head on replication-transcription conflicts of the CCW replisome (39). Utilizing custom microfluidics (40) to ensure healthy cell physiology in combination with time-lapse wide-field fluorescence microscopy, we quantitatively investigate chromosomal replication and segregation during successive cell cycles. We track the replisome by its progression through its components DnaN (the β_2 sliding clamp) and DnaQ (the ε-subunit of DNA polymerase III), and specific chromosomal loci on the left (L) and right (R) replichore arms of the chromosome (Figure 1C). This enables us to investigate the effect of the Tus roadblock on both replication and segregation. Our data indicate that while the Tus–*ter* roadblock impedes replisome progression, the replisome is sufficiently resilient (as assessed from the DNA-bound DnaQ and DnaN molecules) to avoid complete disassembly at the barrier, proceeding to overcome it and finish the replication process in an overall time that only exceeds that of cells with the native origin of replication (*oriC-dnaN*) by 15%. The replication time in the absence of Tus (*oriZ-dnaN:ΔTus* cells) is in excellent agreement with that of *oriC-dnaN* cells, confirming that the Tus–*ter* complex is indeed the barrier responsible for the increased replication time in *oriZ-dnaN* cells. We found that the generation time of all Δ*Tus* mutants with an ectopic or native origin of replication exceeded that of *oriC-dnaN* cells. We investigated the effect of the Tus–*ter* block on the chromosomal segregation organization, since this pattern is sensitive to fork progression (41,42). The sister chromosome alignment (SCA) patterns after replication for the *oriZ-dnaN* and *oriZ-dnaN:ΔTus* cells were found to differ: SCA patterns changed from a predominant Left-Right-Left-Right (LRLR) (*oriZ-dnaN* cells) configuration to a RLLR configuration (*oriZ-dnaN:ΔTus* cells). This suggests that the RFB caused by the Tus–*ter* complex can influence the manner in which the sister chromosomes are segregated and positioned following replication. Collectively, our results show that the replisome is stable, or rapidly restarts after having encountered a natural impediment in the cell. It does not collapse completely but rather remains DNA-bound and overcomes this barrier, possibly with assistance from other proteins.

MATERIALS AND METHODS

The details regarding the experimental procedures can be found in the Supplementary Data. Here we briefly highlight the different strains and techniques used in this study.

Strains, strain construction and growth for microscopy

All endogenous chromosomal integration of the *lacO* and *tetO* arrays, and fusions of either YPet-DnaN, LacI-mCherry and TetR-mCerulean where constructed in previous work and described in detail (38). All chromosomal deletions of the *tus* gene in the different strains were realized by λ-Red recombination and P1 phage transduction.

Cells used for microscopy were grown in M9-Gly supplemented with the necessary nutrients until an OD∼0.2 was reached. The cells were immobilized for imaging using a custom microfluidic system made from polydimethylsiloxane (40). Fresh growth medium was continuously injected automatically into the device during an experiment at 0.5 ml/h via a syringe pump.

Microscopy and image analysis

All microscopy experiments where conducted on a commercial Nikon Ti microscope with custom laser excitation. YPet was imaged using a 515 nm (Cobolt Fandango) laser, mCherry was imaged using a 561 nm (Cobolt Jive) laser and mCerulean was imaged using a 457 nm (Cobolt Twist) laser. The type of extended time-lapse microscopy that we conduct using microfluidics allows us to quantitatively compare intensities since the rate of photobleaching is constant, and hence a steady-state between bleaching and protein products is reached rapidly into the measurement (43). Image acquisition was performed with an EMCCD (Andor) using commercial Nikon NIS elements software. The whole microscope body, including sample, was kept at ∼37 °C using a temperature controller (Okolabs). Image analysis was performed using ImageJ and custom written Matlab code.

RESULTS

Delineating the time when the CW replisome encounters a Tus–*ter* complex from the non-permissive side

We utilize time-lapse fluorescence microscopy in combination with a custom-built microfluidic device (40) to track the independent replisomes and chromosomal loci during chromosomal replication. The individual replisomes are visualized via a functional YPet-DnaN chromosomal fusion (38), and the left- and right replichore arms are imaged using a fluorescent-repressor-operator system (FROS) (44). FROS enables one to image chromosomal loci by engineering binding sites at a defined location on the chromosome to which specific proteins bind. If these proteins are fluorescentely tagged, one then visualize that locus of the chromosome in the form of a focus. The *lacO* array (*ori1*) is posi-

tioned on the left arm, 15 kb CCW from the former position of *oriC*, and the *tetO* array (*R2*) is positioned on the right arm, 21 kb CW of *oriZ* (38) (Figure 1C). Fusions of LacI-mCherry and TetR-mCerulean are expressed at low levels to keep any perturbation to the generation and replication times (45) to a minimum (38,46,47). Kymographs of sample individual cells illustrate the YPet-DnaN and *ori1*-mCherry movements during replication (Figure 2A and B, left). The respective temporal montages of the individual images are shown in the Supplementary Figure S1A and B. We determine the positions of the respective foci for each individual image of a time-lapse measurement by fitting a 1D-Gaussian function across the long axis to the profile summed across the short axis of the bacterium (Supplementary Section 1.7.1). Figure 2A and B (center) depict sample fluorescence images and their corresponding Gaussian fits. The calculated positions per individual image are used to track the YPet-DnaN and *ori1*-mCherry foci over a complete replication cycle in each individual cell. We perform an equivalent analysis to detect and track the *R2*-mCerulean loci (Supplementary Figure S2).

The temporal information of *ori1*-mCherry enables us to establish the moment during replication at which the CW replisome encounters the Tus–*terC* roadblock. This is because the distances of *ori1* from *oriZ* (∼1050 kbp) and of *terC* from *oriZ* (∼1100 kbp) can be seen as equivalent (∼1 Mbp) (Figure 1C). We determine the time-point at which the *ori1*-mCherry focus spatially doubles (Figure 2C). Since the two replisomes are believed to progress at the same rate on average ($v_{\mathrm{rep}} \sim 550$ bp/s) (Supplementary Section 1.8), this time-point is indicative of when the CW replisome encounters the Tus–*terC* roadblock from the non-permissive direction (Figure 2C, inset). The average time following initiation required for the CCW replisome to replicate *ori1* is $t_{ori1} = 26 \pm 6$ min (Error is ± SD; $n = 282$; Figure 2C). This measured time is in agreement with previous measurements (38), as well as with the expected value ($t_{ori1,\,\mathrm{expected}} = 32$ min) calculated using the distance of *ori1* from *oriZ* and the average replication speed (v_{rep}).

A replisome remains DNA-bound after encountering a Tus–*ter* roadblock

Since it is conceivable that the replisome disassembles when encountering a Tus–*ter* complex, we examine the dynamics of the replisome in single cells from initiation till termination, with specific attention given to the time point when the replisome reaches the Tus–*terC* roadblock. Initiation and termination are taken as focus appearance and disappearance. The DNA-bound YPet-DnaN foci are detected and tracked during the whole replication process (Figure 3A, left). The size of the markers in the average time-resolved trace (Supplementary Section 1.7.2) presented is indicative of the percentage of cells at that time point having either a single focus (black dots) or two foci (black circles). The majority of the cells exhibits a single focus at initiation and just prior to termination, while during elongation cells display single and double foci at equal frequencies (Figure 3A, right).

To rule out that the single focus observed in roughly 50% of the cells during elongation results from the CW replisome disassembly at the Tus–*terC* site, we quantify and compare the DNA-bound YPet-DnaN intensity under two conditions. First, we compare the intensity of a single focus (light green) to the sum of the intensity of two foci (dark green) during replication (Figure 3B). We observe only a small difference between the means (<10 %), which suggests that there is no change in the number of DNA-bound YPet-DnaN molecules regardless of whether one or two foci are detected. Thus, the differing number of foci detected does not reflect replisome disassembly, but likely results from occasional DNA conformational changes that result in sufficiently close proximity (below the resolution limit imposed by diffraction) of the two replisome to preclude their separate identification.

Secondly, we establish whether the CW replisome is disassembled after encountering the Tus–*ter* roadblock. This is accomplished by comparing the intensity of DNA-bound YPet-DnaN prior (gray) and post (red) doubling of the *ori1*-mCherry focus (as assessed by the appearance of a second focus, Figure 3C). This comparison is performed by summing the intensities of all the frames prior or post *ori1*-mCherry focus doubling, respectively (similar results are obtained when taking smaller numbers of frames into account, see Supplementary Table S1). We only detect slight differences (<10 %). This implies that there is no significant decrease in the number of DNA-bound YPet-DnaN before and after the replisome has encountered the Tus–*terC* region. This suggests that the replisome, as assessed from the YPet-DnaN signal, remains DNA-bound after encountering a Tus–*ter* roadblock and is not directly disassembled.

Since the sliding clamp has been shown to accumulate on the DNA (43), and is thus not necessarily always bound in the immediate vicinity of the replication fork, we also studied the fate of a different replisome component that is active at the fork: the ε-subunit of DNA polymerase III (DnaQ-YPet). We observed no obvious difference in the number of DnaQ-YPet foci prior and post reaching the Tus–*terC* roadblock, and only a minor difference (<6 %) in the number of DNA-bound DnaQ-YPet, as assessed by comparing the foci intensities before and after the replisome has encountered the Tus–*terC* region (Supplementary Figure S3). These observations, together with the YPet-DnaN measurements, are in-line with the replisome remaining bound (or quickly restarting) after encountering the Tus–*ter* block.

A replisome is impeded by a Tus–*ter* complex, but not halted indefinitely

We demonstrate that the replisome does not only remain DNA bound, but is capable of progressing past the Tus–*ter* block and continues replication. While the replisome does not disassemble following the encounter with Tus–*terC*, it could potentially stall there without further replication; in other words, it is plausible that the CCW replisome synthesizes the remainder of the chromosome while the CW replisome is halted. To test whether the CW replisome can continue replication after having reached the Tus–*terC* block, we compare the replication and division times of *oriZ-dnaN* cells to that of *oriC-dnaN* cells (Table 1). The *oriC-dnaN* cells have a division time of $t_{\mathrm{div},oriC-dnaN} = 85 \pm 15$ min, and *oriZ-dnaN* cells have a $t_{\mathrm{div},oriZ-dnaN} = 97 \pm 21$ min (errors

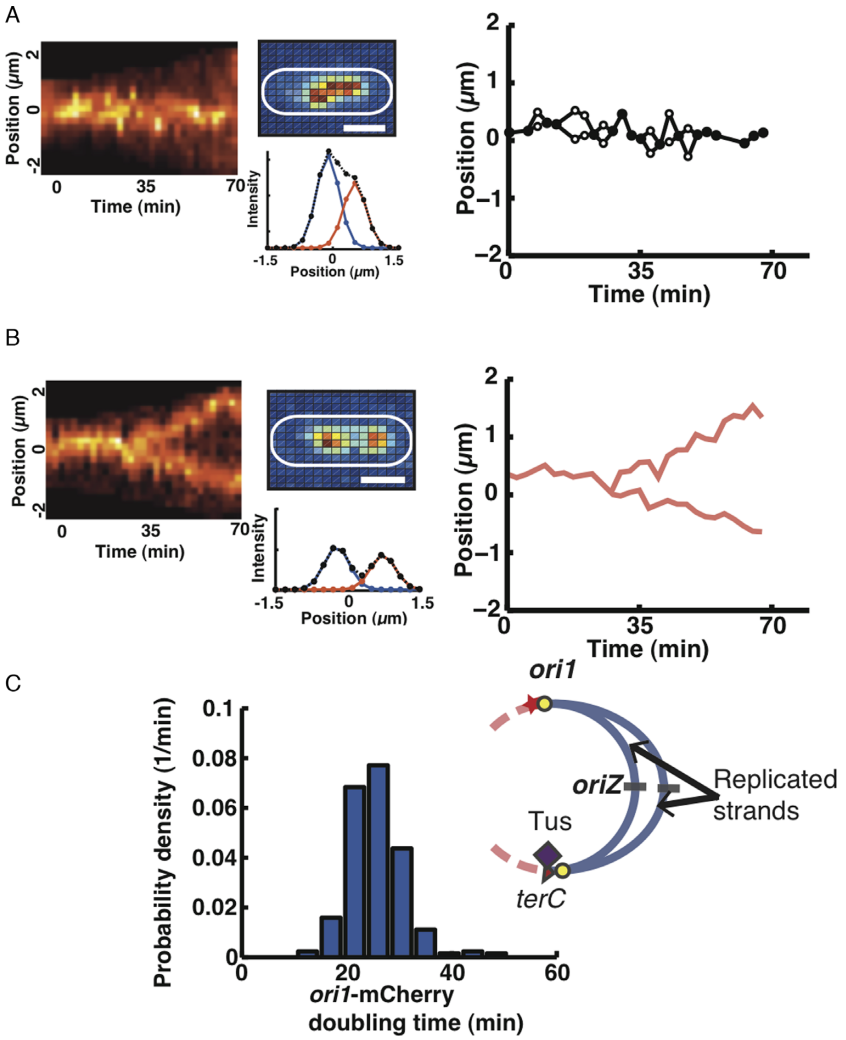

Figure 2. An example individual replication cycle of *oriZ-dnaN* cells. (**A** and **B**) Representative DnaN-YPet and *ori1*-mCherry fluorescent signals. (A and B, left) Individual kymographs of the replisome (Ypet-DnaN) and *ori1*-mCherry locus for one complete replication cycle constructed by summation of the pixel intensities along the short axis of the cell. The replisomes remain relatively close together, while the *ori1*-mCherry loci segregate and move to opposite cell poles. (A and B, center) Sample fluorescent foci of Ypet-DnaN and *ori1*-mCherry imaged (represented here in pseudo-color) together with the their respective Gaussian fits. Scale bars, 1.3 μm. (A and B, right) The complete YPet-DnaN (A, right) and *ori1*-mCherry (B, right) traces shown in (A, left) and (B, left) determined from the Gaussian fitted positions from individual images for each time point. Here, a single YPet-DnaN focus is indicated in a filled circle and two individual foci are indicated as open circles. The lines between data points are included to aid the reader. *ori1*-mCherry positions over time are indicated with solid red lines. (**C**) The distribution of the time point during replication when the *ori1*-mCherry focus doubles. The mean spatial doubling time of the *ori1*-mCherry focus is $t_{ori1} = 26 \pm 6$ min (Error is ± SD, $n_{\text{cells}} = 282$). Here $t = 0$ is taken as initiation of replication. (Inset) We schematically that when ori1-mCherry focus is reached it is indicative of the time point when the CW replisome reaches the Tus–*terC* complex.

are ± SD; Figure 3D, brown). These relatively long division times result from the minimal growth medium (Supplementary Section 1.2) used in the experiments. Thus the division time for *oriZ-dnaN* cells compared to that of *oriC-dnaN* cells increases by ∼13%. The *oriC-dnaN* cells have a replication time of $t_{\text{rep},oriC-dnaN} = 70 \pm 7$ min (errors are ± SD; Supplementary Figure S4A and B). The measured replication time in *oriZ-dnaN* cells is $t_{\text{rep},oriZ-dnaN} = 81 \pm 15$ min (mean ± SD; Figure 3D). If the CW replisome was halted indefinitely, one would expect the CCW replisome to copy ∼1/4 more of the chromosome. This should cause the replication time in *oriZ-dnaN* cells to increase by a factor of 1.5, thus to ∼105 min, a value that notably exceeds the observed increase of ∼1.15×. Even though we cannot fully exclude from our data that the CCW replisome might speed up during replication due to an increased availability of deoxyribonucleotide triphosphates (dNTPs) (48) by the stalling of the CW fork, we deem this to not be the dominant factor, since it has recently been shown that the CW replisome can pass a Tus–*ter* barrier (39). This conclusion is supported by the observation that the number of DNA-bound DnaQ-YPet molecules appears unchanged when the replisome encounters the Tus–*ter* barrier (Supplementary Figure S3). Thus, the marginal increase of the replication time suggests that the CW fork is, at least in a large fraction of the cases, capable of passing the Tus–*terC* block. Given the wide distribution of replication times in *oriZ-dnaN* cells (Figure 3D), it is possible that there was variation in the pausing

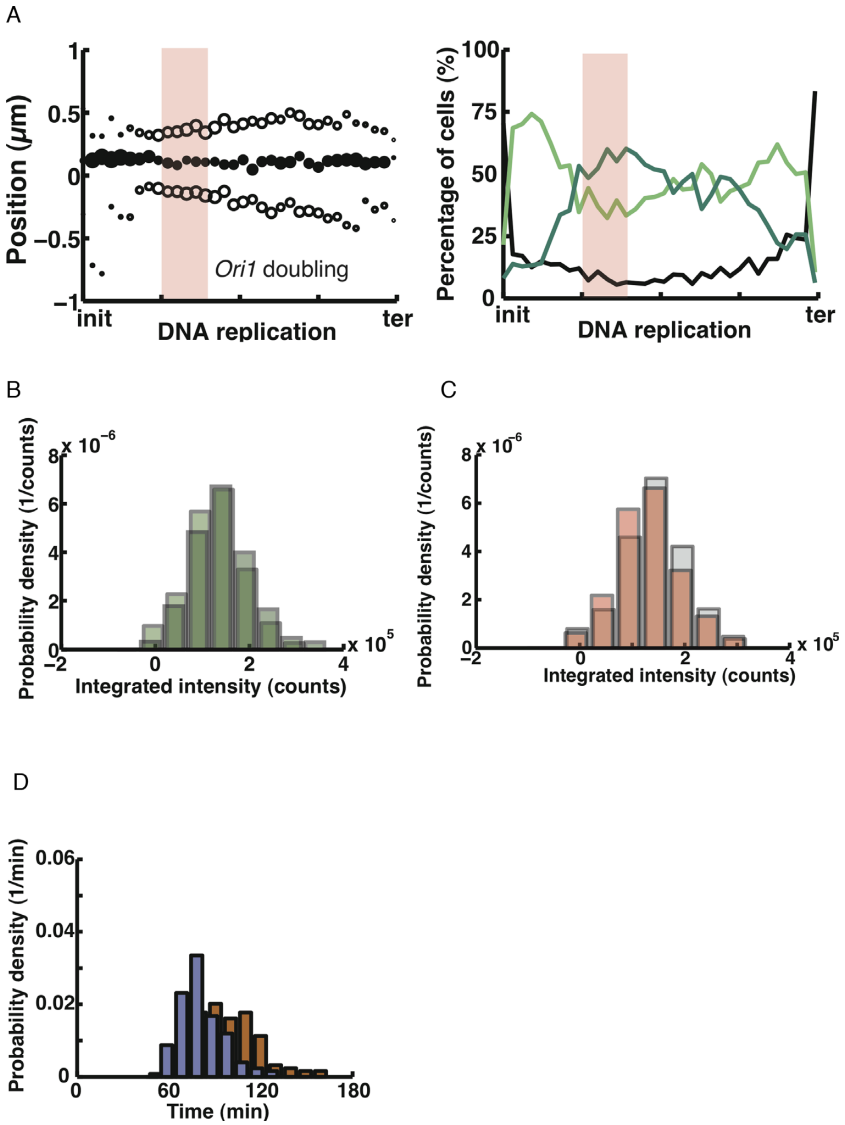

Figure 3. The replisome is slowed down at a Tus–*ter* roadblock, but not halted indefinitely. (**A**) Average replisome behavior during replication in the *oriZ-dnaN*-strain. (left) An average time resolved trace of the two replisomes (YPet-DnaN) from individual cells during complete replication cycles ($n_{\text{cells}} = 128$). Here we plot the single DnaN-YPet focus (filled circles) and double DnaN-YPet foci (open circles). The size of an individual element at each time point is representative of the percentage of cells having that particular distribution of foci. The traces have been aligned with respect to initiation and termination, and binned. The transparent red rectangle indicates the time when *ori1*-mCherry focus spatially doubles, as determined from the distribution in Figure 2C. The width of the rectangle is ± SD. (right) The percentage of cells that have a single focus (light green line), double foci (dark green line) and no foci (black line) as function of replication time. It is evident that the percentage of cells having a single focus or double foci is roughly equally distributed. (**B**) The integrated intensity when only a single YPet-DnaN focus (light green) is visible ($I_{\text{single}} = 1.28 \cdot 10^5 \pm 6.11 \cdot 10^4$), ($n_{\text{foci}} = 2123$), is essential the same as the sum of two individual YPet-DnaN foci (dark green) ($I_{\text{double}} = 1.41 \cdot 10^5 \pm 6.72 \cdot 10^4$), ($n_{\text{foci}} = 1647$). The difference between the two means of the individual distributions is < 10%. This intensity similarity implies that the same number of YPet-DnaN molecules are DNA-bound when a single focus or two foci are detected. (**C**) The intensity distributions of DNA-bound YPet-DnaN prior (gray) and post (red) spatial doubling of the *ori1*-mCherry focus. $I_{\text{prior},ori1-mCherry} = 1.43 \cdot 10^5 \pm 6.58 \cdot 10^4$ counts ($n_{\text{foci}} = 1304$), $I_{\text{post},ori1-mCherry} = 1.31 \cdot 10^5 \pm 6.28 \cdot 10^4$ counts (mean ± SD, $n_{\text{foci}} = 3157$). The difference between the means of the two distributions is < 9%. The number of DNA-bound YPet-DnaN is thus practically unchanged after *ori1*-mCherry has been replicated, i.e. after the CW replisome has encountered the Tus–*terC* roadblock. This unchanged intensity value is indicative of replisomes not being disassembled after encountering a Tus–*ter* roadblock but rather remaining DNA-bound. (**D**) The distribution of the replication times (purple) and the division time (brown) of individual *oriZ-dnaN* cells. The average replication time is $t_{\text{rep},oriZ-dnaN} = 81 \pm 15$ min and the average division time is $t_{\text{div},oriZ-dnaN} = 97 \pm 21$ min (Error is ± SD).

times of individual replisomes upon their encounter with the Tus–Ter barriers. Bridging of such a barrier could well be a stochastic process as opposed to a uniformly regulated one.

Replisome progression is influenced by the absence of Tus in *oriZ-dnaN* cells

To verify that the longer replication time observed in *oriZ-dnaN* cells can be attributed to hampering of the CW replisome by the Tus–*ter* complex, we investigate the replisome dynamics and replication time in *oriZ-dnaN* cells that do not express Tus (*oriZ-dnaN:ΔTus*) (49) (Supplementary Section 1.1.5). This strain is incapable of forming the Tus–*ter* complex, and hence the replisome should be able to progress unimpeded beyond the innermost terminus region.

Double foci are more frequently observed during elongation in *oriZ-dnaN:ΔTus* cells compared to *oriZ-dnaN* cells. A sample trace (Figure 4A) and its corresponding temporal montage (Supplementary Figure S1C and D) illustrate this effect that foci appear to overlap less frequently in *oriZ-dnaN:ΔTus* cells compared to *oriZ-dnaN* cells. The average time-resolved trace (Figure 4B, top) clearly shows that the fraction of cells displaying a single focus during elongation has decreased by a factor of ∼2 (Figure 4B, bottom). This is most likely due to the influence of the absence of the Tus–*ter* roadblock on the replication-dependent chromosome dynamics and organization (41,42).

OriZ-dnaN:ΔTus cells exhibit very similar replication times to *oriC-dnaN* cells. The replication time for *oriZ-dnaN:ΔTus* cells is $t_{\mathrm{rep},oriZ-dnaN\Delta Tus} = 68 \pm 7$ min (Figure 4C), which is consistent with the above argument that the longer replication time in *oriZ-dnaN* cells compared to *oriC-dnaN* cells is due to the Tus–*ter* block. The replication time of *oriZ-dnaN:ΔTus* cells is in close similarity with the replication time for *oriC-dnaN* cells ($t_{\mathrm{rep},oriC-dnaN} = 70 \pm 7$ min) (Supplementary Figure S4B). While the replication time for *oriZ-dnaN:ΔTus* cells is decreased compared to that of *oriZ-dnaN* cells where we found $t_{\mathrm{rep},oriZ-dnaN} \sim 81$ min, the division time is slightly longer $t_{\mathrm{div},oriZ-dnaN\Delta Tus} = 109 \pm 18$ min (Figure 4C) compared to $t_{\mathrm{div},oriZ-dnaN} \sim 97$ min.

To gain further insight into the effect on the replication and division times in the absence of Tus, we investigated these times in *oriC-dnaN* cells that did not express Tus (*oriC-dnaN:ΔTus*) (Supplementary Section 1.1.3; Figure S4). We observed a slight increase in both the division time ($t_{\mathrm{div},oriC-dnaN:\Delta Tus} = 96 \pm 19$ min) and the replication time ($t_{\mathrm{rep},oriC-dnaN:\Delta Tus} = 80 \pm 11$ min) compared to *oriC-dnaN* cells where we found $t_{\mathrm{rep},oriC-dnaN} \sim 70$ min and $t_{\mathrm{div},oriC-dnaN} \sim 85$ min (Supplementary Figure S4C). This increase might be due to the more collision-prone fork fusion in the absence of Tus. No visible difference was observed in the replisome dynamics in terms of single or double foci as function of replication time (Supplementary Figure S4D and E). The division- and replication times of the four different strains have been summarized in Table 1.

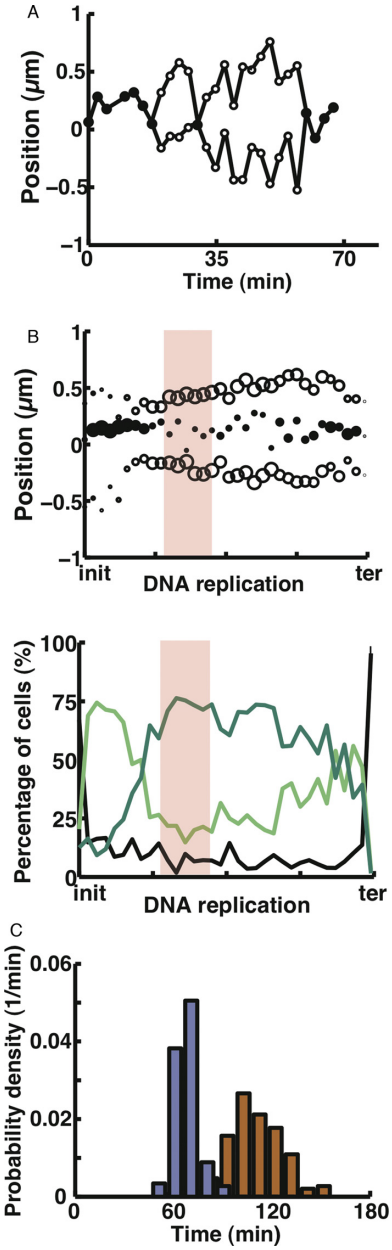

Figure 4. Removing the Tus–*ter* roadblock directly affects replication in oriZ-dnaN:ΔTus cells. (**A**) A representative complete single replication cycle in a single *oriZ-dnaN:ΔTus* cell. A single YPet-DnaN focus is indicated with a solid black dot and two individual foci are indicated as circles. The lines between data points are included to aid the reader. (**B**, top) An average time resolved trace of the two replisomes (YPet-DnaN) from individual cells during complete replication cycles ($n_{\mathrm{cells}} = 152$). Single DnaN-YPet focus are represented as filled cicrcles and double DnaN-YPet foci with open circles. The size of an individual element at each time point is again representative of the percentage of cells having that particular foci distribution. The traces have been aligned with respect to initiation and termination and binned. (bottom) The percentage of cells that have a single focus (light green line), double foci (dark green line) and no foci (black line) as function of replication time. It is evident that the majority of the cells have two foci for the largest part of the replication process. The transparent red rectangle indicates the time when *ori1*-mCherry replicates, as determined from the distribution in Figure 2C. The width of the rectangle is ±SD. (**C**) The distribution of the replication time (purple) and division time (brown) of individual *oriZ-dnaN*:ΔTus cells. The average replication time is $t_{\mathrm{rep},oriZ-dnaN:\Delta Tus} = 68 \pm 7$ min, and the average division time is $t_{\mathrm{div},oriZ-dnaN:\Delta Tus} = 109 \pm 18$ min (Error is ± SD).

Table 1. The division- and replication times together with the respective D-periods for the different *E. coli* strains investigated

E. coli strain	Division time (min)	Replication time (min)	D-period (min)
oriC-dnaN	85 ± 15	70 ± 7	23 ± 9
oriC-dnaN:ΔTus	96 ± 19	80 ± 11	30 ± 13
oriZ-dnaN	97 ± 21	81 ± 15	19 ± 13
oriZ-dnaN:ΔTus	109 ± 18	68 ± 7	31 ± 10

The numbers specified indicate the mean ± SD. Here the replication time is defined as the time interval between YPet-DnaN focus appearance and disappearance. The D-period is defined as the time interval between YPet-DnaN focus disappearance and cell division. The true replication time and the D-period are likely slightly shorter than the reported values, since termination occurs prior to the complete disappearance of a focus. *t*-tests were performed to compare the division- and replication times of the various strains to those of oriC-dnaN. In all the cases the null hypothesis, which states that samples came from normal distributions with equal means was rejected ($P < 0.05$) except in the case of the replication time for oriZ-dnaN:ΔTus ($P = 0.09$).

The presence and absence of Tus influences the sister chromosome alignment pattern in *oriZ-dnaN* cells

To gain more insight into the discernibility of the individual replisomes during replication we investigate the chromosome organization in *oriZ-dnaN* and *oriZ-dnaN:ΔTus* cells. Utilizing the labeled chromosomal loci on the left (*ori1*-mCherry) and right (*R2*-mCerulean) replichores, we visualize their movement during replication (Figure 5A and B). It is evident from the time-resolved traces that the *ori1*-mCherry and *R2*-mCerulean loci segregate and move to opposite cell halves in both cases. The times when the *ori1*-mCherry focus and *R2*-mCerulean focus spatially double are indicated. Since we did not observe a significant difference in the spatial doubling times of the respective loci in the two strains, we grouped the *oriZ-dnaN* and *oriZ-dnaN:ΔTus* data for better statistics. As stated previously, the time measured for the spatial doubling of *ori1* foci ($t_{ori1} = 26 \pm 6$ min) is in excellent agreement with the expected value. In the case of *R2*, one would expect this region to be replicated ∼1 min after initiation given its position and the average speed of a replisome, but we measure $t_{R2} = 17 \pm 5$ min (Error is ± SD, $n = 167$) (Supplementary Figure S2B), in agreement with previous measurements (38). However, this discrepancy between the measured and expected time when *R2* separates, can be attributed to the region of the chromosome that remains juxtaposed for ∼10 min and not yet segregated fully (4,50,51). The pattern at the end of replication between the two strains appears to be different (Figure 5A and B).

The SCA patterns formed illustrate a change in chromosome organization in the absence of Tus. Since the movement or stagnation of the replication fork influences chromosome segregation organization (42,52), we investigated the resulting arrangement of the left (L) and right (R) replichore loci after termination in both the *oriZ-dnaN* and *oriZ-dnaN:ΔTus* cells (Figure 5C). The three segregation patterns observed are LRRL (Figure 5C, left), RLLR (Figure 5C, center), and LRLR (Figure 5C, right). In a minority of the cells (<9 %), the loci of the LR replichore arms spatially overlap (Supplementary Figure S5A), preventing their proper classification. Such cells are discarded from further analysis. The small number of cells displaying a RLRL pattern (Supplementary Figure S5B) are grouped with the LRLR (conform convention, since it is a symmetric configuration (53)). The majority of the *oriZ-dnaN* cells displayed a LRLR pattern, consistent with what has been measured previously (38), while the predominant pattern in *oriZ-dnaN:ΔTus* cells is RLLR. There is thus a switch in the predominant SCA pattern in the absence of Tus. This predominate RLLR pattern is already observed half way through replication (Supplementary Figure S5C). The fraction of *oriZ-dnaN:ΔTus* cells displaying RLLR is larger when determined half way through replication compared to at termination, while for *oriZ-dnaN* cells it is essentially unaffected. Through some mechanism the cell is able to revert back, but not fully, to the 'normal' LRLR pattern.

Fork fusion in *oriZ-dnaN* cells most likely occurs close to *terF*

The time point at which the CW replisome reaches *terC* and the total replication time provide us with insight into the genomic position where termination occurs in *oriZ-dnaN* cells. Since we demonstrated that the CW replisome is not likely disassembled at Tus–*terC*, and that it likely continues synthesis (39,54), albeit being slowed down, it is possible to determine the most likely termination position using the average values for the replication termination time (∼81 min), the time when the CW encounters *terC*, and the replisome speed. From the average time when the CW replisome encounters *terC* (∼26 min), one can calculate that there remain ∼55 min for the two replisomes to copy the remainder (∼2300 kbp) of the genome (Figure 6A). The CCW replisome is not impeded as it synthesizes in the natural direction and would thus progress on average for ∼1800 kbp, assuming a constant velocity of $v \sim 550$ bp/s. This implies that the CW replisome is effectively hampered by the Tus–*ter* barriers for ∼30 min, and replicates ∼500 kbp on average. From this it follows that replication termination, i.e. fork fusion, occurs close to *terF*. However, the distribution of replication times (Figure 3D) also indicates that there are events where termination might occur between *terB*-*terF* (Figure 6B). To illustrate this more quantitatively, we plot the distribution of the time differences between the averaged temporal occurrence of *ori1* spatial doubling and individual replication termination events (Figure 6C). The proportion of cells that terminates faster than ∼55 min is more likely indicative of *terB*-*terF* termination events, while the proportion of cells that terminates after ∼55 min is more likely associated with *terB*/*C* termination events. These proportions are consistent with *terB* and *terC* being strong roadblocks that reduce the rate of CW replisome progression.

Since the CW replisome moves more slowly due to the Tus–*ter* barriers, one might have expected unloading of sliding clamps, resulting in a reduction of their number from the steady-state equilibrium (43). This is not observed, implying

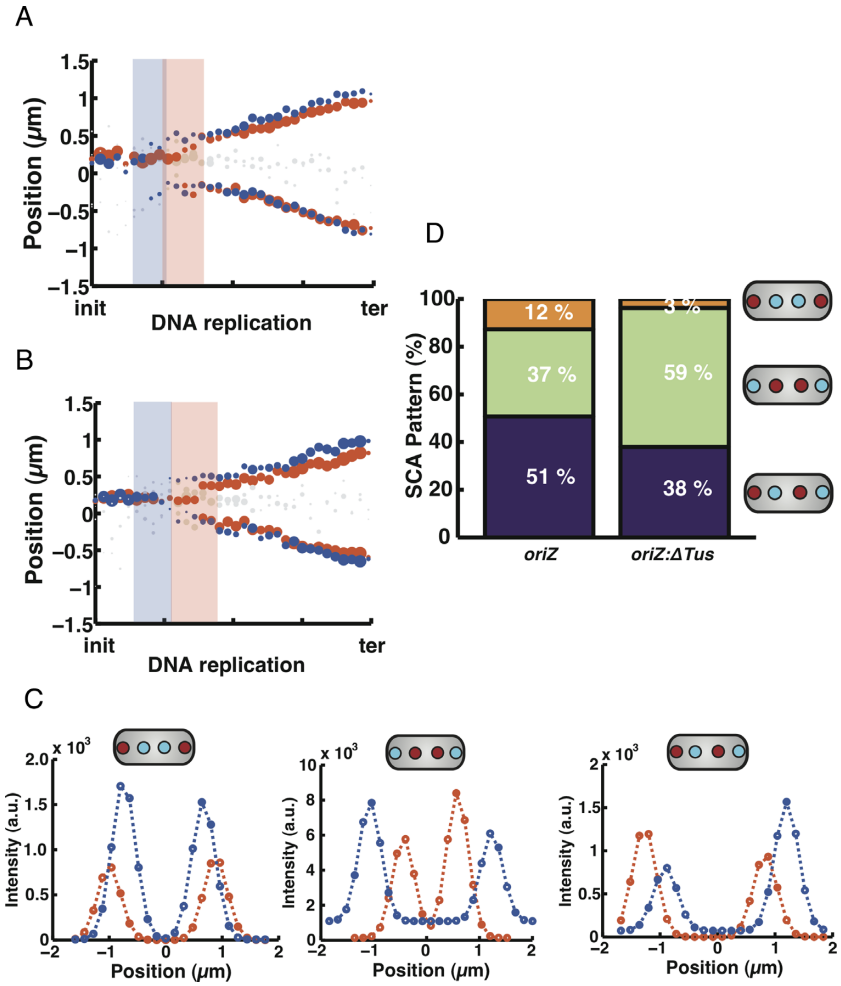

Figure 5. Sister chromosome alignment (SCA) patterns are different for *oriZ-dnaN* and *oriZ-dnaN:ΔTus* cells. (**A** and **B**) Average time resolved traces of the *ori1*-mCherry (red) and *R2*-mCerulean (blue) loci. The blue and red rectangles indicates the time when the respective loci replicate as determined from the distributions in Figure 2C and Supplementary Figure S2. The shaded white dots are when only a single focus was detected, which was in the minority of cases. As with the previous figures, the size of the dots are representative of the percentage of cells having that particular foci distribution. The width of the shaded region is the SD. (**A**) *oriZ-dnaN*-strain ($n_{cells} = 71$). (**B**) *oriZ-dnaN:ΔTus*-strain ($n_{cells} = 79$). (**C**) Example SCA patterns of the left (L) and right (R) replichores after replication. Here we plot the fitted spatial intensity distributions. (left) LRRL, (centre) RLLR and (right) RLRL. (Insets) Schematic depiction of the different chromosomal loci patterns. (**D**) The distributions of the different SCA patterns for the *oriZ-dnaN*- and *oriZ-dnaN:ΔTus*-cells after replication. The predominant pattern for *oriZ-dnaN* (51 %) is the LRLR organization, while for *oriZ-dnaN:ΔTus* cells this is the RLLR organization (59 %). The differences observed in the SCA patterns of the two strains are judged to be significant as evaluated by a chi-square test, which yielded a $\chi^2 = 5.79$ with $P = 0.055$.

that the dynamics of the sliding clamps may be altered in the terminus region in this strain, possibly due to the chromosome compaction of the highly prevalent MatP/matS site specific system that organizes the terminus region (55).

DISCUSSION

To ensure the accurate inheritance of genetic material one needs faithful completion of replication and chromosome segregation. Our work provides insight into the replisome's robustness *in vivo* and into its ability to circumvent the natural Tus–*ter* replication barriers. We characterize the effect of the Tus–*ter* complex on the stability and progression of the replisome when it encounters the barrier from the non-permissive side. Our data suggest that the CW replisome (as assessed by studying YPet-DnaN and DnaQ-Ypet foci) does not disassemble after having encountered the Tus–*terC* complex from the non-permissive direction, but rather remains stably bound to the DNA (or is rapidly reloaded). This result is consistent with what has been observed *in vitro* during a head-on collision of the *E. coli* replisome and an RNA polymerase (RNAP) (36). We observed that the progression of the CW fork is impeded, but that it is capable of overcoming this barrier, as deduced from the unaffected numbers of DNA-bound YPet-DnaN and DnaQ-YPet before and after encountering the roadblock (Figure 3C), together with the fact that the overall replication time only increased by 15% (Figure 3D). Our results are in agreement with a recent study where it was shown, in their strain with only an ectopic origin of replication (*ΔoriC oriZ*), that termination frequently occurs at *terB*, thus the CW replisome crosses the Tus–*terC* barrier (39).

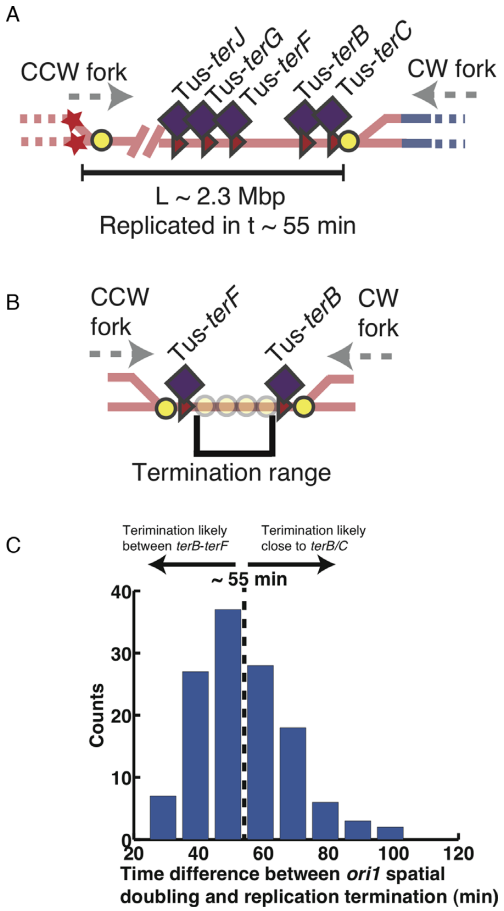

Figure 6. The CW replisome crosses *terB* and *terC*. (**A**) Schematic illustration of the remaining portion of the chromosome that needs to be replicated once the CW replisome has encountered the Tus–*terC* roadblock. (**B**) Zoom-in on the positions at which termination is observed to occur in *oriZ-dnaN* cells. Here the transparent yellow circles are representative of the uncertainty in the exact position of fork position, i.e. termination. (**C**) Distribution of the time differences between the averaged temporal occurrence of *ori1* spatial doubling and individual replication termination events. The dotted line indicates a time difference of 55 min. Time differences smaller than 55 min are consistent with termination occurring in between *terF* and *terB*, while longer time differences are consistent with more substantial halting of the CW fork and hence termination occurring closer to *terB*/*C*.

We demonstrate that the presence and absence of Tus affects the replication- and cell generation-times in both *oriC-dnaN* and *oriZ-dnaN* cells. For both *oriZ-dnaN:ΔTus* and *oriC-dnaN:ΔTus*, an increase in the mean cell doubling time was observed when compared to *oriC-dnaN* and *oriZ-dnaN* cells respectively (∼11 and ∼12%, respectively). In both cases this increase could result from processing events required to complete replication when the converging forks fuse at sites other that Tus-bound *ter* sites. This hypothesis is supported by our observation that there is an increase in the D-period for these strains (Table 1). We note that the replication time for *oriZ-dnaN:ΔTus* was in very good agreement with *oriC-dnaN* cells, strengthening the view that the Tus–*ter* complexes caused the measured replication fork delay in *oriZ-dnaN* cells. We observed a slightly longer replication time for *oriC-dnaN:ΔTus* cells compared to *oriC-dnaN* cells (∼14% increase). This observation of longer replication times in *oriC-dnaN* is in accordance with the RFT model (21,34) that fork fusion and completion of replication is most effective at Tus-bound *ter* sites (56), rather than at the *dif*-site as has been proposed by bioinformatics analysis (57). The *dif* locus, located between *terA* and *terC*, is where the XerCD recombinase decatenates newly replicated sister chromosomes and resolves chromosome dimers of nascent daughter chromosomes to allow successful chromosome segregation (58). If fork fusion occurred at the *dif*-site most frequently, the absence of Tus should have had negligible effect on the replication and cell division. We propose that Tus–*ter* sites around the *dif*-site facilitate the localization of the proteins necessary for proper dimer resolution by ensuring that only one of the two replisomes replicate the *dif* sequence, as postulated by *Duggin et al*. (21). Possibly, fork fusion and attendant collision processes in the direct vicinity of the *dif*-site might influence for example decatenation or dimer resolution, and hence increase the overall duration of replication and cell division.

We observed a switch in the predominant SCA patterns after replication when the *tus* gene was deleted from *oriZ-dnaN* cells. The predominant SCA pattern in *oriC-dnaN* and *oriZ-dnaN* cells has been shown to be LRLR (38). We indeed observed this pattern for *oriZ-dnaN* cells, while interestingly the predominant pattern switched to RLLR in the absence of Tus (*oriZ-dnaN:ΔTus* cells), an organization pattern that is associated with fork stalling (42). One would rather have anticipated that the proportion of cells displaying LRLR pattern should increase when Tus is absent from the cells; since no replication fork stalling is occurring due to Tus–*ter* complexes. Our different observation may imply that the collision of the CW replisome with different proteins after passing the *dif*-site plays a role in the final SCA in *oriZ-dnaN* cells.

A future topic of study would be to investigate the mechanistic details by which the replication fork can progress beyond an RFB caused by the Tus–*ter* complex. The β_2 sliding clamps have been shown to facilitate in bypassing of replication barriers (59). This might be a strategy by which the replisome bridges such an RFB when encountering the Tus–*ter* complex from the permissive side. An Single-strand DNA-binding protein (SSB) for example might facilitate repair at these collisions (60) and in that way assist the replisome. It might be other non-replicative helicases that dispose of these roadblocks (61). For example the *E. coli* helicase II (UvrD) is a 3′ to 5′ helicase that has been shown to be able to remove Tus *in vitro* (62). It is plausible that it could remove Tus from a *ter* site *in vivo* as well. The FtsK translocase involved in chromosome segregation (63,64) is another potential candidate for Tus removal, though a recent single-molecule *in vitro* study has shown that FtsK changes direction when encountering Tus and does not seem to dislodge it from the DNA (65). Independently of which proteins assist the replisome in encountering a roadblock, our work demonstrates that the replisome is robust in continuing replication despite this hurdle.

SUPPLEMENTARY DATA

Supplementary Data are available at NAR Online.

ACKNOWLEDGEMENTS

We thank Christian Lesterlin for support with the *oriZ*-strain, Theo van Laar for stimulating discussions. We thank Jelle van der Does, Dimitri de Roos and Jaap Beekman for their contribution toward instrumentation and infrastructure.

Author Contributions: M.C.M. and N.H.D. designed the research. M.C.M., S.T.K. and N.H.D. designed the experiments. S.T.K. undertook the experiments. R.d.L and V.L assisted during experiments and contributed to discussions. S.T.K. constructed strains. M.C.M. and J.W.J.K. wrote software to analyze the microscopy data. M.C.M. and J.W.J.K. analyzed the data. D.J.S. provided strains and contributed to the discussion of the work. M.C.M., R.d.L and N.H.D wrote the paper.

FUNDING

Wellcome Trust Program Grant [WT083469 to D.J.S.]; European Community's Seventh Framework Programme FP7/2007-2013 [241548 (MitoSys) to N.H.D.]; Netherlands Organisation for Scientific Research (NWO) Vici grant (to N.H.D.). Funding for open access charge: European Community's Seventh Framework Programme FP7/2007-2013 [241548 (MitoSys)]; Netherlands Organisation for Scientific Research (NWO) Vici grant.

Conflict of interest statement. None declared.

REFERENCES

1. Johnson,A. and O'Donnell,M. (2005) Cellular DNA replicases: components and dynamics at the replication fork. *Annu. Rev. Biochem.*, **74**, 283–315.
2. McHenry,C.S. (2011) DNA replicases from a bacterial perspective. *Annu. Rev. Biochem.*, **80**, 403–436.
3. Duderstadt,K.E., Reyes-Lamothe,R., van Oijen,A.M. and Sherratt,D.J. (2013) Replication-Fork Dynamics. *Cold Spring Harb. Perspect. Biol.*, **6**, 1–17.
4. Reyes-Lamothe,R., Possoz,C., Danilova,O. and Sherratt,D.J. (2008) Independent positioning and action of Escherichia coli replisomes in live cells. *Cell*, **133**, 90–102.
5. Jun,S. and Wright,A. (2010) Entropy as the driver of chromosome segregation. *Nat. Rev. Microbiol.*, **8**, 600–607.
6. Kuwada,N.J., Cheveralls,K.C., Traxler,B. and Wiggins,P.A. (2013) Mapping the driving forces of chromosome structure and segregation in Escherichia coli. *Nucleic Acids Res.*, **41**, 7370–7377.
7. Di Ventura,B., Knecht,B., Andreas,H., Godinez,W.J., Fritsche,M., Rohr,K., Nickel,W., Heermann,D.W. and Sourjik,V. (2013) Chromosome segregation by the Escherichia coli Min system. *Mol. Syst. Biol.*, **9**, 686.
8. Fisher,J.K., Bourniquel,A., Witz,G., Weiner,B., Prentiss,M. and Kleckner,N. (2013) Four-dimensional imaging of E. coli nucleoid organization and dynamics in living cells. *Cell*, **153**, 882–895.
9. Youngren,B., Nielsen,H.J., Jun,S. and Austin,S. (2014) The multifork Escherichia coli chromosome is a self-duplicating and self-segregating thermodynamic ring polymer. *Genes Dev.*, **28**, 71–84.
10. Merrikh,H., Zhang,Y., Grossman,A.D. and Wang,J.D. (2012) Replication-transcription conflicts in bacteria. *Nat. Rev. Microbiol.*, **10**, 449–458.
11. Michel,B., Grompone,G., Florès,M.-J. and Bidnenko,V. (2004) Multiple pathways process stalled replication forks. *Proc. Natl. Acad. Sci. U.S.A.*, **101**, 12783–12788.
12. Gupta,M.K., Guy,C.P., Yeeles,J.T.P., Atkinson,J., Bell,H., Lloyd,R.G., Marians,K.J. and McGlynn,P. (2013) Protein-DNA complexes are the primary sources of replication fork pausing in Escherichia coli. *Proc. Natl. Acad. Sci. U.S.A.*, **110**, 7252–7257.
13. Hill,T.M., Tecklenburg,M.L., Pelletier,A.J. and Kuempel,P.L. (1989) tus, the trans-acting gene required for termination of DNA replication in Escherichia coli, encodes a DNA-binding protein. *Proc. Natl. Acad. Sci. U.S.A.*, **86**, 1593–1597.
14. Hidaka,M., Kobayashi,T., Takenaka,S., Takeya,H. and Horiuchi,T. (1989) Purification of a DNA replication terminus (ter) site-binding protein in Escherichia coli and identification of the structural gene. *J. Biol. Chem.*, **264**, 21031–21037.
15. Hill,T.M. (1992) Arrest of bacterial DNA replication. *Annu. Rev. Microbiol.*, **46**, 603–633.
16. Coskun-Ari,F.F., Skokotas,A., Moe,G.R. and Hill,T.M. (1994) Biophysical characteristics of Tus, the replication arrest protein of Escherichia coli. *J. Biol. Chem.*, **269**, 4027–4034.
17. Rudolph,C.J., Upton,A.L., Briggs,G.S. and Lloyd,R.G. (2010) Is RecG a general guardian of the bacterial genome? *DNA Repair*, **9**, 210–223.
18. Hill,T.M. and Marians,K.J. (1990) Escherichia coli Tus protein acts to arrest the progression of DNA replication forks in vitro. *Proc. Natl. Acad. Sci. U.S.A.*, **87**, 2481–2485.
19. Bidnenko,V., Ehrlich,S.D. and Michel,B. (2002) Replication fork collapse at replication terminator sequences. *EMBO J.*, **21**, 3898–3907.
20. Neylon,C., Kralicek,A.V., HILL,T.M. and Dixon,N.E. (2005) Replication termination in Escherichia coli: structure and antihelicase activity of the Tus-Ter complex. *Microbiol. Mol. Biol. Rev.*, **69**, 501–526.
21. Duggin,I.G., Wake,R.G., Bell,S.D. and Hill,T.M. (2008) The replication fork trap and termination of chromosome replication. *Mol. Microbiol.*, **70**, 1323–1333.
22. Kaplan,D.L. and Bastia,D. (2009) Mechanisms of polar arrest of a replication fork. *Mol. Microbiol.*, **72**, 279–285.
23. Mulcair,M.D., Schaeffer,P.M., Oakley,A.J., Cross,H.F., Neylon,C., Hill,T.M. and Dixon,N.E. (2006) A molecular mousetrap determines polarity of termination of DNA replication in E. coli. *Cell*, **125**, 1309–1319.
24. Bastia,D., Zzaman,S., Krings,G., Saxena,M., Peng,X. and Greenberg,M.M. (2008) Replication termination mechanism as revealed by Tus-mediated polar arrest of a sliding helicase. *Proc. Natl. Acad. Sci. U.S.A.*, **105**, 12831–12836.
25. Berghuis,B.A., Dulin,D., Yu,Z., van Laar,T., Cross,B., Janissen,R., Jergic,S., Dixon,N.E., Depken,S. and Dekker,N.H. (2015) Strand separation suffices to establish a long-lived, foolproof DNA-protein lock at the Tus-Ter replication fork barrier. *Nat. Chem. Biol.*, **11**, 579–585.
26. Gottlieb,P.A., WU,S., Zhang,X., Tecklenburg,M., Kuempel,P. and Hill,T.M. (1992) Equilibrium, kinetic, and footprinting studies of the Tus-Ter protein-DNA interaction. *J. Biol. Chem.*, **267**, 7434–7443.
27. Neylon,C., Brown,S.E., Kralicek,A.V., Miles,C.S., Love,C.A. and Dixon,N.E. (2000) Interaction of the Escherichia coli replication terminator protein (Tus) with DNA: a model derived from DNA-binding studies of mutant proteins by surface plasmon resonance. *Biochemistry*, **39**, 11989–11999.
28. Lewis,P.J., Ralston,G.B., Christopherson,R.I. and Wake,R.G. (1990) Identification of the replication terminator protein binding sites in the terminus region of the Bacillus subtilis chromosome and stoichiometry of the binding. *J. Mol. Biol.*, **214**, 73–84.
29. Bussiere,D.E., Bastia,D. and White,S.W. (1995) Crystal structure of the replication terminator protein from B. subtilis at 2.6 A. *Cell*, **80**, 651–660.
30. Lemon,K.P., Kurtser,I. and Grossman,A.D. (2001) Effects of replication termination mutants on chromosome partitioning in Bacillus subtilis. *Proc. Natl. Acad. Sci. U.S.A.*, **98**, 212–217.
31. Willis,N.A., Chandramouly,G., Huang,B., Kwok,A., Follonier,C., Deng,C. and Scully,R. (2014) BRCA1 controls homologous recombination at Tus/Ter-stalled mammalian replication forks. *Nature*, **510**, 556–559.
32. Larsen,N.B., Sass,E., Suski,C., Mankouri,H.W. and Hickson,I.D. (2014) The Escherichia coli Tus-Ter replication fork barrier causes site-specific DNA replication perturbation in yeast. *Nat. Commun.*, **5**, 3574.
33. Hill,T.M., Henson,J.M. and Kuempel,P.L. (1987) The terminus region of the Escherichia coli chromosome contains two separate loci that exhibit polar inhibition of replication. *PNAS*, **84**, 1754–1758.
34. Duggin,I.G. and Bell,S.D. (2009) Termination structures in the Escherichia coli chromosome replication fork trap. *J. Mol. Biol.*, **387**, 532–539.

35. Moreau,M. J.J. and Schaeffer,P.M. (2012) Differential Tus-Ter binding and lock formation: implications for DNA replication termination in Escherichia coli. *Mol. Biosyst.*, **8**, 2783–2791.
36. Pomerantz,R.T. and O'Donnell,M. (2010) Direct restart of a replication fork stalled by a head-on RNA polymerase. *Science*, **327**, 590–592.
37. Yeeles,J.T.P. and Marians,K.J. (2011) The Escherichia coli replisome is inherently DNA damage tolerant. *Science*, **334**, 235–238.
38. Wang,X., Lesterlin,C., Reyes-Lamothe,R., Ball,G. and Sherratt,D.J. (2011) Replication and segregation of an Escherichia coli chromosome with two replication origins. *Proc. Natl. Acad. Sci. U.S.A.*, **108**, E243–E250.
39. Ivanova,D., Taylor,T., Smith,S.L., Dimude,J.U., Upton,A.L., Mehrjouy,M.M., Skovgaard,O., Sherratt,D.J., Retkute,R. and Rudolph,C.J. (2015) Shaping the landscape of the Escherichia coli chromosome: replication-transcription encounters in cells with an ectopic replication origin. *Nucleic Acids Res.*, **43**, 7865–7877.
40. Moolman,M.C., Huang,Z., Krishnan,S.T., Kerssemakers,J.W.J. and Dekker,N.H. (2013) Electron beam fabrication of a microfluidic device for studying submicron-scale bacteria. *J. Nanobiotechnol.*, **11**, 12.
41. Rocha,E. (2004) The replication-related organization of bacterial genomes. *Microbiology*, **150**, 1609–1627.
42. Liu,X., Wang,X., Reyes-Lamothe,R. and Sherratt,D.J. (2010) Replication-directed sister chromosome alignment in Escherichia coli. *Mol. Microbiol.*, **75**, 1090–1097.
43. Moolman,M.C., Krishnan,S.T., Kerssemakers,J.W.J., van den Berg,A., Tulinski,P., Depken,M., Reyes-Lamothe,R., Sherratt,D.J. and Dekker,N.H. (2014) Slow unloading leads to DNA-bound β2-sliding clamp accumulation in live Escherichia coli cells. *Nat. Commun.*, **5**, 5820.
44. Wang,X., Reyes-Lamothe,R. and Sherratt,D.J. (2008) Visualizing genetic loci and molecular machines in living bacteria. *Biochem. Soc. Trans.*, **36**, 749–753.
45. Possoz,C., Filipe,S.R., Grainge,I. and Sherratt,D.J. (2006) Tracking of controlled Escherichia coli replication fork stalling and restart at repressor-bound DNA in vivo. *EMBO J.*, **25**, 2596–2604.
46. Wang,X., Possoz,C. and Sherratt,D.J. (2005) Dancing around the divisome: asymmetric chromosome segregation in Escherichia coli. *Genes Dev.*, **19**, 2367–2377.
47. Wang,X., Liu,X., Possoz,C. and Sherratt,D.J. (2006) The two Escherichia coli chromosome arms locate to separate cell halves. *Genes Dev.*, **20**, 1727–1731.
48. Morigen Odsbu,I. and Skarstad,K. (2009) Growth rate dependent numbers of SeqA structures organize the multiple replication forks in rapidly growing Escherichia coli. *Genes Cells*, **14**, 643–657.
49. Roecklein,B., Pelletier,A. and Kuempel,P. (1991) The tus gene of Escherichia coli: autoregulation, analysis of flanking sequences and identification of a complementary system in Salmonella typhimurium. *Res. Microbiol.*, **142**, 169–175.
50. Wang,X., Reyes-Lamothe,R. and Sherratt,D.J. (2008) Modulation of Escherichia coli sister chromosome cohesion by topoisomerase IV. *Genes Dev.*, **22**, 2426–2433.
51. Joshi,M.C., Bourniquel,A., Fisher,J., Ho,B.T., Magnan,D., Kleckner,N. and Bates,D. (2011) Escherichia coli sister chromosome separation includes an abrupt global transition with concomitant release of late-splitting intersister snaps. *Proc. Natl. Acad. Sci. U.S.A.*, **108**, 2765–2770.
52. Nielsen,H.J., Youngren,B., Hansen,F.G. and Austin,S. (2007) Dynamics of Escherichia coli chromosome segregation during multifork replication. *J. Bacteriol.*, **189**, 8660–8666.
53. Wang,X., Montero Llopis,P. and Rudner,D.Z. (2013) Organization and segregation of bacterial chromosomes. *Nat. Rev. Genet.*, **14**, 191–203.
54. Mettrick,K.A. and Grainge,I. (2015) Stability of blocked replication forks in vivo. *Nucleic Acids Res.*, **44**, 657–668.
55. Mercier,R., Petit,M.A., Schbath,S., Robin,S. and El Karoui,M. (2008) The MatP/matS site-specific system organizes the terminus region of the E. coli chromosome into a macrodomain. *Cell*, **135**, 475–485.
56. Rudolph,C.J., Upton,A.L., Stockum,A., Nieduszynski,C.A. and Lloyd,R.G. (2013) Avoiding chromosome pathology when replication forks collide. *Nature*, **500**, 608–611.
57. Hendrickson,H. and Lawrence,J.G. (2007) Mutational bias suggests that replication termination occurs near the dif site, not at Ter sites. *Mol. Microbiol.*, **64**, 42–56.
58. Lesterlin,C., Barre,F.-X. and Cornet,F. (2004) Genetic recombination and the cell cycle: what we have learned from chromosome dimers. *Mol. Microbiol.*, **54**, 1151–1160.
59. Georgescu,R.E., Yao,Y.N. and O'Donnell,M. (2010) Single-molecule analysis of the Escherichia coli replisome and use of clamps to bypass replication barriers. *FEBS Lett.*, **584**, 2596–2605.
60. Shereda,R.D., Kozlov,A.G. and Lohman,T.M. (2008) SSB as an organizer/mobilizer of genome maintenance complexes. *Crit. Rev. Biochem. Mol. Biol.*, **43**, 289–318.
61. Boubakri,H., de Septenville,A.L., Viguera,E. and Michel,B. (2010) The helicases DinG, Rep and UvrD cooperate to promote replication across transcription units in vivo. *EMBO J.*, **29**, 145–157.
62. Hiasa,H. and Marians,K.J. (1992) Differential inhibition of the DNA translocation and DNA unwinding activities of DNA helicases by the Escherichia coli Tus protein. *J. Biol. Chem.*, **267**, 11379–11385.
63. Sherratt,D.J., Arciszewska,L.K. and Crozat,E. (2010) The Escherichia coli DNA translocase FtsK. *Biochem. Soc.*, **38**, 395–398.
64. Grainge,I. (2013) Simple topology: FtsK-directed recombination at the dif site. *Biochem. Soc. Trans.*, **41**, 595–600.
65. Lee,J.Y., Finkelstein,I.J., Arciszewska,L.K., Sherratt,D.J. and Greene,E.C. (2014) Single-molecule imaging of FtsK translocation reveals mechanistic features of protein-protein collisions on DNA. *Mol. Cell*, **54**, 832–843.
66. Kamada,K., Horiuchi,T., Ohsumi,K., Shimamoto,N. and Morikawa,K. (1996) Structure of a replication-terminator protein complexed with DNA. *Nature*, **383**, 598–603.